

# PIC simulation of a strong double layer in a nonrelativistic plasma flow: Electron acceleration to ultrarelativistic speeds

Mark E. Dieckmann<sup>1</sup>

*Department of Science and Technology (ITN), Linköping University, SE-60174 Norrköping, Sweden*  
and

Antoine Bret

*ETSI Ind., Universidad de Castilla-La Mancha, 13071 Ciudad Real, Spain*

Mark.E.Dieckmann@itn.liu.se

## ABSTRACT

Two charge- and current neutral plasma beams are modelled with a one-dimensional PIC simulation. The beams are uniform and unbounded. The relative speed between both beams is  $0.4c$ . One beam is composed of electrons and protons and one out of protons and negatively charged oxygen (dust). All species have the temperature 9 keV. A Buneman instability develops between the electrons of the first beam and the protons of the second beam. The wave traps the electrons, which form plasmons. The plasmons couple energy into the ion acoustic waves, which trap the protons of the second beam. A proton phase space hole grows, which develops through its interaction with the oxygen and the heated electrons into a rarefaction pulse. This pulse drives a strong ion acoustic double layer, which accelerates a beam of electrons to about 50 MeV, which is comparable to the proton kinetic energy. The proton distribution eventually evolves into an electrostatic shock. Beams of charged particles moving at such speeds may occur in the foreshock of supernova remnant shocks. This double layer is thus potentially relevant for the electron acceleration (injection) into the diffusive shock acceleration by supernova remnants shocks.

*Subject headings:* physical data and processes: acceleration of particles — physical data and processes: plasmas — methods: numerical

## 1. Introduction

The blast shell of a supernova remnant (SNR) can accelerate charged particles to cosmic ray energies through diffusive shock acceleration by the SNR shocks (Uchiyama et al. 2007; Reynolds 2008; Hillas 2005). Particles are scattered upstream and downstream of a shock and some particles cross the shock repeatedly, gaining energy each time (Bell 1978; Krymsky 1977; Blandford & Ostriker 1978; Malkov & Drury 2001). Diffusive shock acceleration requires a seed pop-

ulation of particles with energies well in excess of the thermal ones, since only such particles can cross the shock repeatedly and be scattered efficiently by the magnetohydrodynamic waves on either side of the shock. The presence of shock-accelerated electrons is evidenced by the radio emissions of SNRs. It is not clear yet how the electrons can reach the energy threshold for diffusive shock acceleration; that requires that their kinetic energies are comparable to those of the ions. Some electrons must be accelerated locally, that is close to the SNR shock or close to one of its precursors (Reynolds 2008; Hillas 2005).

This injection of electrons is thought to be ac-

---

<sup>1</sup>Visiting researcher at the Centre for Plasma Physics (CPP), Queen's University Belfast, BT7 1NN Belfast, U.K.

complished by the interplay of energetic ions with electrons and dust (Ellison et al. 1997) by means of plasma instabilities (Cargill & Papadopoulos 1988). The instabilities occur in the upstream plasma, just ahead of the SNR shock. This region is called the foreshock. One source of the ion beams is the downstream plasma. Ions can leak through the shock boundary and outrun it (Malkov 1998). The shock can also reflect a substantial fraction of the upstream ions. If the reflection is specular, then the ions can cross the foreshock at twice the shock speed. Reflected and leaked ion beams can be observed in situ at the Earth bow shock (Eastwood et al. 2005). Particle-in-cell (PIC) simulations of fast plasma shocks suggest, that they may also occur at SNR shocks when the upstream magnetic field is orthogonal to the shock normal (Hoshino & Shimada 2002; Lembege et al. 2004; Chapman et al. 2005; Amano & Hoshino 2007). Precursor shocks move ahead of the main SNR shock. They can reach mildly relativistic speeds for the most extreme supernova explosions (Kulkarni et al. 1998). Such shocks can also reflect ions in the presence of a quasi-parallel magnetic field (Dieckmann, Shukla & Drury 2008).

We focus in this work on ion beam instabilities in the foreshock, but we do not model the shock itself. We rely on a foreshock model that has been widely used, e.g. in the works by Shimada & Hoshino (2003, 2004) and by Dieckmann et al. (2007, 2008a). This model considers an ion beam, which moves through the upstream plasma, consisting of cool electrons and protons. The system is spatially uniform. Often a second, counter-propagating ion beam is introduced, which cancels the current of the first one. This second beam can be due to ions that have been reflected by a perpendicular shock and which return to the shock, after they have been rotated by the upstream magnetic field (McClements et al. 1997). Here a beam of co-moving negatively charged oxygen ions cancels the current of a proton beam.

This foreshock model can be used if all processes develop on scales well below an ion Larmor radius and an inverse ion cyclotron frequency in the case of a perpendicular shock. The foreshock model may be representative over larger scales otherwise, because ions can expand much

farther if they move along the magnetic field, as it is observed at the Earth’s bow shock. This foreshock model is not self-consistent, because it decouples the foreshock physics from that of the shock. It also assumes a plasma that is spatially uniform, while the shock reflected ion beams vary in their mean speed and temperature. However, we can examine with this model the acceleration of the upstream electrons as a function of the bulk parameters, such as the beam temperatures and mean speeds and the background magnetic field. We can also separate individual processes from the global shock dynamics, that involves coupling over many scales (Hoshino 2003). This simplifies their identification and interpretation. The periodic boundary conditions also allow us to reduce the box size, making PIC simulations computationally efficient even for realistic ion-to-electron mass ratios. The insight gained from such simulations can then guide us in the selection of plasma parameters for the more realistic and demanding PIC simulations of full shocks.

Simulation studies employing this foreshock model have revealed that proton beam-driven instabilities are not efficient electron accelerators. An obstacle is the mass difference between the electrons and the protons. Most plasma instabilities saturate by accelerating the electrons. The fields are too weak to accelerate the ions and the heated electrons quench most of the known plasma instabilities, e.g. through Landau damping. Often only a few per cent of the ion energy is transferred to the electrons (Shimada & Hoshino 2003, 2004; Dieckmann et al. 2007, 2008a). Initially, this is also the case for ion beams that expand into the upstream plasma (Dieckmann et al. 2008b) prior to the formation of a shock. Certain mechanisms (Kuramitsu & Krasnoselskikh 2005; Katsouleas & Dawson 1983) can, in principle, accelerate the electrons to relativistic speeds, but this remains yet to be demonstrated with self-consistent PIC simulations. However, the electrons, that have been accelerated by an instability like the Buneman instability (BI) (Buneman 1958), are often spatially bunched, for example in form of phase space holes (Roberts & Berk 1967; Korn & Schamel 1996a,b; Dieckmann et al. 2007). Electron bunches or plasmons have a much higher inertia than electrons and they modulate the ions to give ion acoustic waves. The ion acoustic waves

can trigger further processes, one of which we consider in this work.

We investigate a plasma consisting of two spatially uniform beams. One beam is composed of protons and electrons and the second one of protons and oxygen carrying a single negative charge. Each of the beams is charge and current neutral. Both beams move at a relative speed of  $0.4c$ . All species have the temperature 9 keV. These initial conditions are the simplest ones that take into account three particle species and they permit a first assessment of the impact of heavier ions. Section 2 discusses in more detail these initial conditions and their potential relevance for a foreshock plasma. Section 3 describes the simulation results, which can be summarized as follows. A BI develops between the electrons and the protons of the second beam. The BI saturates by forming electron phase space holes and these plasmons feed wave energy into the ion acoustic wave (Mendonca & Bingham 2002; Mendonca et al. 2005). Proton phase space holes develop, once the ion acoustic waves are strong enough to trap the beam protons. The electrons eventually thermalize and they reach a mildly relativistic thermal speed, which is stabilizing the system for some time. The BI plays no further role after the electron thermalization. We examine in detail a proton phase space hole that grows into being a proton density pulse with a negative density (Infeld et al. 1989; Infeld & Rowlands 1990). The growth of this proton phase space hole may be caused by its interaction with the negative oxygen (Eliasson & Shukla 2004) or by the disruption of the electron current (Smith 1982). The pulse triggers a strong ion acoustic double layer and it evolves subsequently into an electrostatic shock. The electron phase space structure and evolution of this double layer resembles that, found by a recent simulation study by Newman et al. (2001). That study addressed the electron acceleration in the Earth’s auroral ionosphere. However, our simulation yields the much stronger electron acceleration that is necessary for injecting the electrons into the diffusive shock acceleration at SNR shocks. The proton phase space distribution also differs from the standard picture of double layers outlined, for example, in the review papers by Smith (1982) and by Raadu & Rasmussen (1988). The trapped and free streaming protons in our

simulation are well-separated in velocity, which is not generally the case for double layers. The substantial free energy stored in the difference of the mean velocities of both beams causes the extreme electron acceleration up to 50 MeV. We discuss our simulation results in section 4, we relate it to previous investigations of double layers and we discuss the necessary future research.

## 2. The initial conditions and the simulation method

The bulk plasma of a supernova blast shell can expand into the ambient medium at a speed of up to  $0.1c$ - $0.2c$ , at least during its early phase (Vink et al. 2006; Fransson et al. 2002). A fraction of the blast shell plasma may expand even faster. A plasma flow speed of  $0.9c$  has, for example, been observed for a subshell ejected by a particularly violent supernova explosion (Kulkarni et al. 1998). Shocks form where the expanding plasma impacts on the ambient plasma, the interstellar medium. The typical shock speeds should be comparable to the few per cent of  $c$  the main blast shell plasma has, but some precursor shocks may be considerably faster. The detailed structure in particular of the fastest SNR shocks is unclear. We assume here, that the foreshock region is resembling at least qualitatively that of the well-known Earth bow shock (Eastwood et al. 2005) and we focus on the ion foreshock. The ion foreshock is characterized by the presence of ion beams that can propagate far into the upstream.

However, we expect that a hot background of electrons is present in the foreshock, as PIC simulations of mildly relativistic shocks demonstrate (Dieckmann, Shukla & Drury 2008).

We examine the interaction between two spatially uniform and unbounded plasma beams, consisting of one negatively and one positively charged species each. One beam consists of electrons and protons and the second one of protons and oxygen carrying a single negative charge.

The simulation box frame is the reference frame, in which both plasma beams move in opposite  $x$ -directions and with equal speed moduli  $v_b$ . The simulation models only the  $x$ -direction, which allows us to resolve simultaneously the ion scales and the electron scales at the correct mass ratio.

The beam 1 consists of electrons with the plasma frequency  $\Omega_e = (e^2 n_e / m_e \epsilon_0)^{1/2}$ , where  $e$  and  $n_e$  are the elementary charge and the electron number density and  $\epsilon_0$  is the dielectric constant. The equally dense protons have the plasma frequency  $\Omega_p = R_p^{1/2} \Omega_e$ , where  $R_p = m_e / m_p$ . Both species move at the mean speed  $\langle v \rangle = -v_b$  with  $v_b = c/5$ . The beam 2 is composed of protons with  $\Omega_p$  and oxygen, which carries a single negative charge. The oxygen plasma frequency is  $\Omega_o = \Omega_p/4$ . The mean speed of both species of beam 2 is  $\langle v \rangle = v_b$ . All species have the temperature  $T = 9.1$  keV, which gives the electron thermal speed  $v_e = (k_B T / m_e)^{0.5} = v_b / 1.5$ . By neglecting the  $T \neq 0$  and the heavy species of each beam, the dispersion relation for the beam-aligned electrostatic modes can be cast into the form

$$1 - \frac{\Omega_e^2}{(\omega + k v_b)^2} - \frac{\Omega_p^2}{(\omega - k v_b)^2} = 0. \quad (1)$$

The wavenumber and frequency in the reference frame of beam 1 of the most unstable wave are  $k_u = \Omega_e / 2v_b$  and  $\omega_u = \Omega_e$ . The Doppler-shift will reduce the frequency of the most unstable wave to  $\Omega_e/2$ . The wavelength  $\lambda_u = 2\pi/k_u$ . The phase speed  $v_{ph} = \omega_u/k_u \approx 2v_b$  in the reference frame of beam 1 or  $v_b$  in the box frame. Replacing the oxygen with electrons gives symmetric beams, which lets the phase speed of the waves vanish in the box frame. An exact resonance between the plasmons and the proton beam would not be possible. The estimates for  $\omega_u$  and  $k_u$ , as well as the growth rate  $\Omega_{BC}/\Omega_e \approx (3^{1/2}/2^{4/3})(\Omega_p/\Omega_e)^{2/3} \approx 0.056$  of the cold BI (Buneman 1958) are fairly accurate. Figure 1 shows the numerically obtained growth rate  $\Omega_B/\Omega_e$  for our plasma parameters. This growth rate map has been obtained by using a warm fluid model (Bret et al. 2008). The growth rate map is symmetric around  $v_b$ , so we do not need to consider  $k_y$ . The growth rate in the warm plasma model is lower than in the cold one by about 10%. The corresponding wave number is increased by 20%. The growth rate decreases for increasing  $k_z$ .

The PIC simulation method Dawson (1983) solves the Vlasov-Maxwell set of equations with the method of characteristics. It approximates the phase space density  $f(\mathbf{x}, \mathbf{v}, t)$  by an ensemble of computational particles (CPs). The CPs correspond to phase space volume elements and are not

physical particles. The charge  $q_{cp}$  and mass  $m_{cp}$  of a CP can thus differ from those of the particles it represents. The charge-to-mass ratio  $q_{cp}/m_{cp}$  must, however, equal that of the physical particles and the ensemble properties of the CPs approximate well those of the physical plasma. The trajectories of the CPs are prescribed by the Lorentz equation of motion. The Maxwell-Lorentz set of equations can be normalized, which provides us with results that are independent of the plasma density.

Let  $e$  and  $m_e$  be the elementary charge and the electron mass.

Our code is based on the numerical scheme outlined by Eastwood (1991) and it solves the Maxwell's equations for all components of the electromagnetic fields together with the Lorentz equation, which updates the three-dimensional vector of the relativistic momentum for an ensemble of computational particles (CPs).

The relevance of double layers for solar and astrophysical particle acceleration has been proposed first by Alfven & Carlquist (1967). Lembege & Dawson (1989) have found double layers with PIC simulations of oblique shocks, which dissipated the electron energy. In our PIC simulation the double layer emerges out of the BI and prior to the formation of the shock. A relativistic and monoenergetic electron beam is ejected by the double layer. The time evolution of the proton pulse implies, that the mean energy of this beam rises in time to about 50 MeV, which is a much stronger acceleration than that reported, for example, for previous PIC simulations of double layers (Sato & Okuda 1980).

The nonrelativistic beam speed and the high temperature ensure that the BI grows fastest. The approximation of this system by a 1D PIC simulation, which enforces a monodirectional (plane) wave spectrum, may thus initially be justified. This geometry and the idealized initial conditions facilitate the interpretation of the physical processes and they permit us to resolve the relevant spatio-temporal scales. However, the growth rate of the oblique modes is not negligible and the wave power is isotropized in time through weak turbulence (Ziebell et al. 2008). The PIC simulation may also become unrealistic when the electrons have been accelerated to relativistic speeds. This is, because of the unresolved higher-dimensional

instabilities, the generation of energetic photons through synchrotron- and bremsstrahlung and the back-reaction of these processes onto the plasma (Weibel 1959; Bret A. 2006; Schlickeiser & Lerche 2007; Schlickeiser 2003; Fleishman & Toptygin 2007).

Charged dust and heavy ions exist in the supernova ejecta and in the interstellar medium (Ellison et al. 1997; Meikle et al. 2006). Their ionization state and their relative densities are unclear. It is typically only the dust, which has a negative time-dependent charge (Momeni et al. 2007; Verheest & Pillay 2008), while the oxygen is positively charged (Katsuda et al. 2008). Our initial conditions are thus not necessarily representative for SNR blast shell plasmas. However, the purpose of the oxygen is to introduce a slower time scale (Eliasson & Shukla 2004) and also to obtain a resonance between plasmons and the ion acoustic wave, which facilitates their coupling (Mendonca & Bingham 2002). Both conditions can probably also be achieved by heavier ions, by a mix of ions or by dust.

The beam speed of  $0.4c$  is too high for typical SNR bulk flows, which can reach about 10-20% of the speed of light  $c$  (Vink et al. 2006; Fransson et al. 2002). However, the shock-reflected ion beams can outrun the shock. Some components of the expanding plasma may also move faster than the mean speed of the SNR ejecta. Precursor shocks of particularly strong SNRs may reach speeds of up to  $0.9c$  (Kulkarni et al. 1998). We select this beam speed, because it facilitates the processes we consider and because it allows us to estimate the maximum energy, which the electrons could gain in typical SNR flows through the plasma instabilities discussed here. The beam speed is also low enough to favor the growth of the BI rather than that of the multi-dimensional filamentation instability (Lee & Lampe 1973).

The simulation box length is  $L \approx 1170\lambda_u$ . It is resolved by  $N_g = 7 \cdot 10^4$  grid cells, each with the length  $\Delta_x \approx 0.31\lambda_D$ . The electron Debye length is  $\lambda_D = v_e/\Omega_e$ . Each of the four species is represented by 250 CPs per grid cell, giving a total of  $N_p = 1.75 \cdot 10^7$  per species. The system is followed in time for  $t_S\Omega_e \approx 2600$ , which is subdivided into  $10^5$  time steps  $\Delta_t$ . The beams propagate the distance  $t_S v_b < L/5$  and even a light pulse can cross  $L$  just once. Effects due to the periodic boundary

conditions of the simulation box can not occur.

### 3. Simulation results

The electrostatic BI develops between the electrons of beam 1 and the protons of beam 2. However, the secondary instabilities give rise to electric fields, which will let all particle species interact. Figure 2 displays the time evolution of the relevant energy densities, which are the energy density  $E_F(t) = \epsilon_0 N_g^{-1} \sum_{j=1}^{N_g} E_x^2(j\Delta_x, t)$  of the electrostatic field and the  $E_i(t) = N_g^{-1} \Delta_x^{-3} \sum_{j=1}^{N_p} m_i c^2 [\Gamma(v_j) - 1]$ , where the summation is over all particles  $j$  of the species  $i$  with the mass  $m_i$  and a speed  $v_j(t)$  giving  $\Gamma(v_j) = (1 - v_j^2/c^2)^{-1/2}$ .

The  $E_F \propto E_x^2$  grows in the interval  $t\Omega_e < 100$  at an exponential rate  $2\Omega_i \approx 0.06$ , which is below  $2\Omega_B = 0.098$ . The growth rate  $\Omega_B$  is calculated for a sine wave. The  $L \gg \lambda_u$  and the broad  $k_x$  spectrum of unstable waves in fig. 1 implies, however, that we integrate over a mixture of waves, all of which have a growth rate  $\leq \Omega_B$  and the initial growth of  $E_F$  cannot be compared directly to  $\Omega_B$ . The electron trapping lets  $E_F(t)$  saturate at  $t\Omega_e \approx 100$  and it causes the growth of  $E_1(t)$ . Thereafter  $E_F(t)$  decreases and reaches a meta-equilibrium at  $t\Omega_e \approx 10^3$ . The  $E_1(t)$  is almost constant until  $t\Omega_e \approx 1500$ , when it and  $E_F(t)$  start to grow again. All ion beams have lost less than 1% of their energy prior to  $t\Omega_e \approx 1500$ , confirming that the BI is not an efficient electron accelerator. Then  $E_2(t)$  and  $E_3(t)$  start to change and even  $E_4(t)$  has decreased by 1% at  $t\Omega_e \approx 2600$ .

Figure 3 shows the phase space distributions of the trapped electrons and of the protons of beam 2 at  $t\Omega_e = 145$  in a subinterval of the simulation box. The trapped electrons gyrate around a potential that is moving with the mean speed  $v_b$  of beam 2, which is also the phase speed of the Buneman wave. Only a fraction of the electrons is trapped. The electrons of the untrapped bulk population move on oscillatory phase space paths. The electron phase space hole in the interval  $0 < x/\lambda_u < 1$  has the expected size, while the electron phase space hole in the interval  $2 < x/\lambda_u < 3.5$  is larger. Electron phase space holes increase their size by coalescence and their mutual interaction will deform them (Roberts & Berk 1967). The mean momentum of the proton beam is weakly

modulated. The initially periodic train of electron phase space holes will coalesce, until only a dissipative equilibrium and solitary electron phase space holes remain (Korn & Schamel 1996a,b).

Figure 4 confirms this. A simulation box interval is selected at the time  $t\Omega_e = 10^3$ , in which an electron depletion at  $x/\lambda_u \approx 9$  separates the turbulent region  $x/\lambda_u < 8$  from a smooth plateau at larger  $x$ . The latter constitutes a dissipative equilibrium. The supplementary movie 1 follows the time-evolution of the electron phase space distribution at the position of the electron depletion. The color scale is the 10-logarithm of the number of CPs. Note that the absolute position in the box is given in movie 1, while fig. 4 uses a relative position. The movie 1 demonstrates that it is this density depletion, which is responsible for the turbulent phase space region. A spatial correlation is visible in the fig. 4 between the electron depletion and a phase space hole in the protons of beam 2. This explains why the electron depletion is stationary in the reference frame of movie 1, which moves with  $v_b$  in the box frame. The electron temperature is now relativistically high, by which the linear damping of the ion acoustic waves is reduced and these modes can accumulate wave energy. The thermal anisotropy of the electrons causes the growth of the Weibel instability (Weibel 1959), but it is suppressed here by the 1D geometry.

Figure 5 plots the  $E_x$ , the density of the proton beam 2 and that of the electrons at the same location and time as fig. 4. The electric field at  $x/\lambda_u \approx 9$  is attractive for the protons and repels the electrons, which is in agreement with the observed phase space structure in fig. 4. The electric field amplitude at this position is not unusually large, while the plasma density depletion is. The oxygen density is unaffected at this time, as we show below.

The component energies in fig. 2 demonstrate that the equilibrium between  $E_F(t)$  and  $E_1(t)$  breaks at  $t\Omega_e \approx 1500$  and that a secondary instability sets in after that time. An examination of the full phase space data shows, that this secondary instability is spatially localized. Two similar, but spatially well-separated structures develop in the phase space distribution of the protons of beam 2 in the box. That two structures rather than one grow suggests, that they develop with a

reasonable probability and that their growth is not accidental. Figure 6 displays the larger of these two structures at  $t\Omega_e = 2000$ . A different sub-interval of the box than in the fig 4 is investigated, since the proton phase space structures convect with  $v_b$ . We refer to this proton structure as a pulse. This pulse constitutes a density depletion (Infeld et al. 1989; Infeld & Rowlands 1990). The supplementary movie 2 animates in time the development of the pulse out of the proton phase space hole. The color scale shows the 10-logarithm of the number of CPs. The movie 2 displays absolute box coordinates and its reference frame moves with  $v_b$  through the box. It demonstrates that the proton phase space hole is stationary for a long time, before it develops into a rapidly growing pulse. It is this pulse that is responsible for the energy changes in the fig 2.

The electron phase space distribution reveals in fig. 6 a double layer that is driven by the pulse. This double layer accelerates on  $5\lambda_u$  a beam of electrons out of the bulk to about 7.5 MeV. The movie 1 demonstrates that the mean energy of the electron beam grows in time, while the beam temperature remains unchanged. The electron beam then interacts with the bulk electrons through a two-stream instability, which is responsible for the large beam momentum oscillations. The electric field of the double layer is strong enough to decrease the mean speed modulus of the proton beam 1, which supplies the energy for the electron acceleration. The movie 2 is stopped, when the protons of beam 1 and 2 start to mix by the formation of an electrostatic shock. The movie 1 is stopped, when the electron beam energy exceeds the one resolved by the movie window.

The electron distribution at  $t\Omega_e = 2600$  is illustrated by fig 7. The double layer has not spatially expanded but the electrons are now accelerated to 50 MeV in the box frame, exceeding even the 20 MeV energy of the protons in the same reference frame. The total density of the ultrarelativistic beam in fig. 7b) is about 40% of the density of the bulk electrons in fig. 7c). The momentum distribution of the bulk electrons is practically identical to that in the fig.4. This ultrarelativistic electron beam would drive the unresolved and faster-growing oblique mode instability (Bret A. 2006), rather than the two-stream instability evidenced by the movie 1. The type of instability should,

however, not be important for the evolution of the electron double layer because it forms well behind it.

Figure 8 displays the phase space distributions of both proton beams in the same spatial interval as fig. 7. The proton distributions of both beams have merged and a large electrostatic shock forms at  $x/\lambda_u \approx 55$ . A second electrostatic shock involving only the protons of beam 2 occurs at  $x/\lambda_u \approx 92$ . The movie 2 illustrates that the second shock is driven by the rapid expansion of the proton density pulse. It is remarkable that some protons of beam 2 have increased their  $p_x$  momentum by a factor 2.6 through the electrostatic field, which is also shown by fig.8. The electron double layer is thus also a proton accelerator. The electrostatic field of the double layer does not change its sign, which contrasts the bipolar fields of phase space holes, like in fig 5.

Solitary phase space holes are typically time-stationary in one dimension (Roberts & Berk 1967; Korn & Schamel 1996a,b) and the question arises, why the proton phase space holes grow here into such powerful rarefaction pulses. The proton phase space hole is stable over a long time and it then suddenly turns into a pulse, which suggests an effect that develops on a slower time scale. The electric field of the proton phase space hole will gradually displace the oxygen ions. Figure 9 displays the density distribution of the oxygen ions at the three times  $t\Omega_e = 1000$ ,  $t\Omega_e = 1600$  and  $t\Omega_e = 2000$ . The frame is moved with the beam 2 and the proton phase space hole is located at  $(x - v_b t) \approx 20$  in the chosen frame. The oxygen depletion at  $t\Omega_e = 10^3$  is comparable to the statistical fluctuations of the number of CPs. The integration of the density over 3 grid cells reduces these statistical fluctuations by the factor  $\sqrt{3}$ , but it keeps the density depletion value unchanged. The proton phase space hole grows into the pulse at  $t\Omega_p \approx 1500$ . Figure 9b) reveals that the oxygen density modulation is significant at around this time. It is thus likely that the sudden growth of the proton phase space hole is a consequence of this oxygen depletion. As the proton pulse grows, the structure and amplitude of the oxygen depletion remain qualitatively unchanged, but the depletion expands in space. This may reflect the observation from the movie 2 that the shape of the proton pulse is practically unchanged until

$t\Omega_e \approx 2000$ . The proton pulse and the oxygen depletion are intertwined.

The proton beam 1 and the electrons in our simulation have a significant mean speed in the reference frame of the proton phase space hole and they could provide the energy for the growth of the proton pulse. The movie 1 reveals that the proton phase space hole gives rise to vortices in the electron phase space distribution and the electron flow is turbulent, which exerts a drag on the proton phase space hole. A coupling between the proton phase space hole and the streaming electrons is established, which can also trigger or accelerate the growth of the phase space hole (Dupree 1986). The simulation further evidences that the proton pulse grows at the expense of the kinetic energy of the proton beam 1.

#### 4. Discussion

This work has examined secondary instabilities triggered by the Buneman instability (BI) (Buneman 1958) with a PIC code (Eastwood 1991). One spatial x-direction has been resolved, which implies that the wave spectrum driven by the BI is monodirectional. This limits the realism of the simulation but it firstly allows us to resolve all relevant spatio-temporal scales and, secondly, it facilitates the identification of the relevant physical processes. The large box has ensured that the periodic boundary conditions have not affected the results. We have considered two unmagnetized, interpenetrating, uniform and unbounded beams that have been composed of three particle species. The beam 1 has contained protons and electrons and the beam 2 has been formed by protons and by oxygen with a single negative charge. Each beam has been charge- and current neutral. The relative speed between both beams has been set to 0.4c and the initial temperature of all species has been selected to be 9.1 keV.

The BI has saturated by the trapping of electrons (Roberts & Berk 1967), which groups the electrons into phase space holes that give rise to charge density modulations. The latter can behave as quasi-particles and are thus referred to as plasmons. We could match the mean (group) speed of these plasmons with that of the protons of beam 2 by selecting negatively charged oxygen rather than electrons. Such a resonance facili-

tates the coupling of the plasmon energy into the ion acoustic wave mode (Mendonca & Bingham 2002).

Initially the equilibrium between the electric fields and the electrons has been preserved (Korn & Schamel 1996a,b) and the ion beams had lost only a small fraction of their energy; the electrons moved consequently only at mildly relativistic speeds. The thermal anisotropy of the electron distribution would trigger an instability similar to that proposed by Weibel (1959), resulting in the growth of magnetic fields and multi-dimensional field structures that cannot be represented by a 1D PIC simulation. The Weibel instability may, however, not be important. The proton phase space holes form simultaneously with the collapse of the electron phase space holes that gives rise to the thermal anisotropy. The electromagnetic fields of the Weibel instability may not be strong enough to affect the interplay between the already present proton phase space holes and the oxygen and might be negligible.

As the time progressed, two large density rarefaction pulses (Infeld et al. 1989; Infeld & Rowlands 1990) have developed in the protons of the beam 2. We have examined the larger one in more detail. The long time between the formation of the proton phase space hole and the pulse has suggested that it has been caused by the oxygen response. We have found that the proton density pulse grows, once the electric field of the proton phase space hole has displaced a substantial fraction of the oxygen ions. A related effect has been observed by Eliasson & Shukla (2004). There it was shown that an electron phase space hole was ejected by a density depletion in the background ions, which its electric fields excavated. Here, the consequence of the oxygen depletion is not the acceleration of the phase space hole but its growth. The electrons may also contribute to the growth of the proton phase space hole (Dupree 1986).

The growth of the proton density pulse has resulted in an electron double layer that accelerated the electrons to ultrarelativistic speeds. To the best of our knowledge this is the first time that such an electron acceleration could be observed in PIC simulations of nonrelativistic beam instabilities. The electrons have reached a peak energy of 50 MeV. This immense electron acceleration implies, that the 1D PIC simulation geometry is not

appropriate any more. Firstly, the electrons moving at such speeds drive the oblique mode instability (Bret A. 2006), rather than the two-stream instability. The oblique modes are excluded by the simulation geometry. Secondly, the extreme electron temperature anisotropy resulting from the thermalization of the ultrarelativistic electron beam would drive a very strong Weibel-type instability. The subsequent magnetic field growth would imply that electrons emit synchrotron radiation on top of the bremsstrahlung (Schlickeiser 2003; Fleishman & Toptygin 2007). The balance of these processes (Schlickeiser & Lerche 2007) requires a three-dimensional geometry and a method to deal with the radiation, which is not possible with our PIC code.

At the same time, this electron double layer constitutes a plasma structure that can easily accelerate the electrons to a speed, which allows them to enter the diffusive shock acceleration mechanism. This could be achieved with beam speeds that are not much higher than the flow speeds of supernova blast shells (Vink et al. 2006; Fransson et al. 2002). The oxygen ions we have modelled can also be found in such plasmas, although not in the high density and in the ionisation number we have assumed here (Katsuda et al. 2008). Our negative charge is more representative of dust, which we also find in supernova blast shells (Meikle et al. 2006). Our findings can thus not be applied directly to a supernova scenario. However, the formation of the electron double layer in the presence of heavier ions clearly demonstrates the need to introduce these into PIC simulations, which so far only consider one ion species (Amano & Hoshino 2007; Chapman et al. 2005).

Future simulation work must address the minimum speed, at which the double layer can form. This has to be done in form of parametric simulation studies, because it is not clear for which combinations of the beam speeds and temperatures the double layers can form. Existing analytic studies (Verheest & Pillay 2008) do not cover the case we consider here. The effects of the obliquely propagating modes driven by the initial beam instability have to be examined, as well as those due to the Weibel instability driven by the thermal anisotropy of the electron distribution after the initial BI has saturated. This requires at least two-dimensional PIC simulations. Finally, other



ion species and plasma compositions have to be examined to assess how easily double layers can form. This is important, because the ion composition is not easily obtained (Ellison et al. 1997) and not unique.

The modelling of double layers and their consequences is also of interest for other astrophysical scenarios. Ion double layers, which are characterized by ion distributions that resemble the electron distribution here, may regulate the mass inflow onto neutron stars (Williams et al. 1986) and accelerate particles in accretion discs (Moslem et al. 2007). They may also contribute to solar coronal ejections (Alfven & Carlquist 1967).

This work has been financially supported by the visiting scientist scheme of the Queen's University Belfast, by the Swedish research council Vetenskapsrådet and by the projects FTN 2003-00721 of the Spanish Ministerio de Educación y Ciencia and PAI-05-045 of the Consejería de Educación y Ciencia de la Junta de Comunidades de Castilla-La Mancha. The Swedish High-Performance Computer Center North (HPC2N) has provided the computer time and support.

## REFERENCES

- Alfven, H. & Carlquist, P. 1967, *Solar Phys.*, 1, 220
- Amano, T. & Hoshino, M. 2007, *ApJ*, 661, 190
- Bell, A. R. 1978, *MNRAS*, 182, 443
- Blandford, R. D. & Ostriker, J. P. 1978, *ApJ*, 221, L29
- Bret, A. 2006, *Europhys. Lett.*, 74, 1027
- Bret, A., Gremillet, L., Benisti, D. & Lefebvre, E. 2008, *Phys. Rev. Lett.*, 100, 205008
- Buneman, O. 1958, *Phys. Rev. Lett.*, 1, 8
- Cargill, P. J. & Papadopoulos, K. 1988, *ApJ*, 329, L29
- Chapman, S. C., Lee, R. E. & Dendy, R. O. 2005, *Space Sci. Rev.*, 121, 5
- Dawson, J. M. 1983, *Rev. Mod. Phys.*, 55, 403
- Dieckmann, M. E., Bret, A. & Shukla P. K. 2007, *Plasma Phys. Controll. Fusion*, 49, 1989
- Dieckmann, M. E., Bret, A. & Shukla, P. K. 2008a, *New J. Phys.*, 10, 013029
- Dieckmann, M. E., Meli, A., Shukla, P. K., Drury, L. O. C. & Mastichiadis, A. 2008b, *Plasma Phys. Controll. Fusion*, 50, 065020
- Dieckmann, M. E., Shukla, P. K. & Drury, L. O. C. 2008, *ApJ*, 675, 586
- Dupree, T. H. 1986, *Phys. Fluids*, 29, 1820
- Eastwood, J. W. 1991, *Comput. Phys. Commun.*, 64, 252
- Eastwood, J.P., Lucek, E. A., Mazelle, C., Meziane, K., Narita, Y., Pickett, J. & Treumann R. A. 2005, *Space Sci. Rev.*, 118, 41
- Eliasson, B. & Shukla, P. K. 2004, *Phys. Rev. Lett.*, 93, 045001
- Ellison, D. C., Drury, L. O. C. & Meyer, J. P. 1997, *ApJ*, 487, 197
- Fleishman, G. D. & Toptygin, I. N. 2007, *Phys. Rev. E*, 76, 017401
- Fransson, C., et al. 2002, *ApJ*, 572, 350
- Hillas, A. M. 2005, *J. Phys. G.*, 31, R95
- Hoshino, M. 2003, *Sci.*, 299, 834
- Hoshino, M. & Shimada N. 2002, *ApJ*, 572, 880
- Infeld, E. & Rowlands, G. 1990, *Phys. Rev. A*, 42, 838
- Infeld, E., Rowlands, G. & Torven, S. 1989, *Phys. Rev. Lett.*, 62, 2269
- Katsouleas, T. & Dawson, J. M. 1983, *Phys. Rev. Lett.*, 51, 392
- Katsuda, S., Mori, K., Tsunemi, H., Park, S., Hwang, U., Burrows, D. N., Hughes, J. P. & Slane, P. O. 2008, *ApJ*, 678, 297
- Korn, J. & Schamel, H. 1996a, *J. Plasma Phys.*, 56, 307
- Korn, J. & Schamel, H. 1996b, *J. Plasma Phys.*, 56, 339

- Kulkarni, S. R., Frail, D. A., Wieringa, M. H., Ekers, R. D., Sadler, E. M., Wark, R. M., Higdon, J. L., Phinney, E. S. & Bloom, J. S. 1998, *Nature*, 395, 663
- Krymsky, G. F. 1977, *Sov. Phys. Dokl.*, 22, 327
- Kuramitsu, Y. & Krasnoselskikh, V. 2005, *Phys. Rev. Lett.*, 94, 031102
- Lee, R. & Lampe, M. 1973, *Phys. Rev. Lett.*, 31, 1390
- Lembege, B. & Dawson, J. M. 1989, *Phys. Rev. Lett.*, 62, 2683
- Lembege, B., et al. 2004, *Space Sci. Rev.*, 110, 161
- Malkov, M. A. 1998, *Phys. Rev. E*, 58, 4911
- Malkov, M. A. & Drury, L. O. 2001, *Rep. Prog. Phys.*, 64, 429
- McClements, K. G., Dendy, R. O., Bingham, R., Kirk, J. G. & Drury, L. O. 1997, *MNRAS*, 291, 241
- Meikle, W. P. S., et al. 2006, *ApJ*, 649, 332
- Mendonca, J. T. & Bingham, R. 2002, *Phys. Plasmas*, 9, 2604
- Mendonca, J. T., Norreys, P., Bingham, R. & Davies, J. R. 2005, *Phys. Rev. Lett.*, 94, 245002
- Momeni, M., Kourakis, I., Moslehi-Fard, M. & Shukla, P. K. 2007, *J. Phys. A*, 40, F473
- Moslem, W. M., Kourakis, I., Shukla, P. K. & Schlickeiser, R. 2007, *Phys. Plasmas*, 14, 102901
- Newman, D. L., Goldman, M. V., Ergun, R. E. & Mangeney, A. 2001, *Phys. Rev. Lett.*, 87, 255001
- Raadu, M. A. & Rasmussen, J. J. 1988, *Astrophys. Space Sci.*, 144, 43
- Reynolds, S. R. 2008, *ARA&A*, 46, 89
- Roberts, K. V. & Berk, H. L. 1967, *Phys. Rev. Lett.*, 19, 297
- Sato, T. & Okuda, H. 1980, *Phys. Rev. Lett.*, 44, 740
- Schlickeiser, R. 2003, *A&A*, 410, 397
- Schlickeiser, R. & Lerche, I. 2007, *A&A*, 476, 1
- Shimada, N. & Hoshino, M. 2003, *Phys. Plasmas*, 10, 1113
- Shimada, N. & Hoshino, M. 2004, *Phys. Plasmas*, 11, 1840
- Smith, R. A. 1982, *Phys. Scripta*, T2/1, 238
- Uchiyama, Y., Aharonian, F. A., Tanaka, T., Takahashi, T. & Maeda, Y. 2007, *Nature*, 449, 576
- Verheest, F. & Pillay, S. R. 2008, *Phys. Plasmas*, 15, 013703
- Vink, J., Bleeker, J., van der Heyden, K., Bykov, A., Bamba, A. & Yamazaki, R. 2006, *ApJ*, 648, L33
- Weibel, E. S. 1959, *Phys. Rev. Lett.*, 2, 83
- Williams, A. C., Weisskopf, M. C., Elsner, R. F., Darbo, W. & Sutherland, P. G. 1986, *ApJ*, 305, 759
- Ziebell, L. F., Gaelzer, R., Pavan, J. & Yoon, P. H. 2008, *Plasma Phys. Contr. Fusion*, 50, 085001

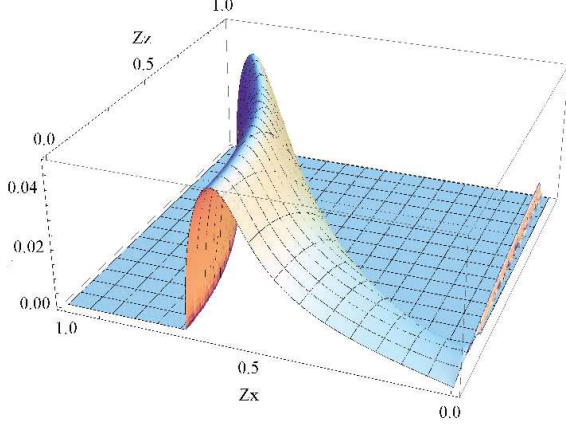


Fig. 1.— The linear growth rate  $\Omega_B/\Omega_e$  is given as the height and as a function of the flow-aligned wavenumber  $Z_x = k_x v_b/\Omega_e$  and one perpendicular  $Z_z = k_z v_b/\Omega_e$ . The growth rate maximum  $\Omega_B/\Omega_e = 0.049$  is found at  $Z_z = 0$  and  $Z_x = 0.59$ , which is close to the  $\Omega_{BC}/\Omega_e = 0.056$  and  $k_u v_b/\Omega_e = 0.5$  of the cold BI.

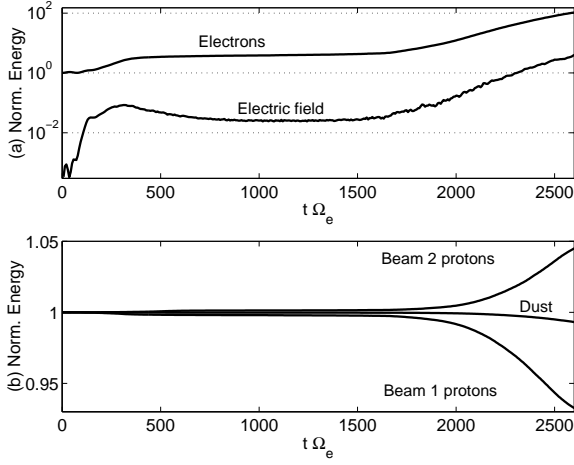


Fig. 2.— The electrostatic energy density  $E_F$  and the kinetic energy densities  $E_i$  of the four particle species  $i$ : Panel a) shows  $E_F$  and the  $E_1$  of the electrons of beam 1, both normalized to  $E_1(t=0)$ . Panel b) plots the  $E_2$  of the protons of beam 1, the  $E_3$  of the protons of beam 2 and the  $E_4$  of the oxygen of beam 2, which are all normalized to their respective initial value.

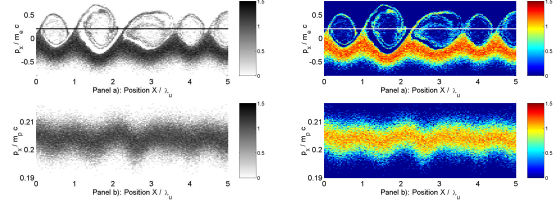


Fig. 3.— The phase space distribution of the electrons (a) and of the protons of beam 2 (b) at  $t\Omega_e = 145$ : The colour scale shows the 10-logarithm of the number of CPs. The electrons form phase space holes, which are coalescing. The horizontal line corresponds to the mean momentum  $v_b/(1-v_b^2/c^2)^{1/2}$  of beam 2. The protons show velocity modulations that are spatially correlated with the electron phase space holes.

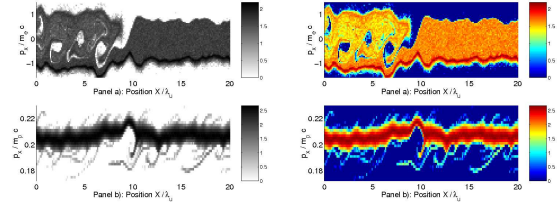


Fig. 4.— The phase space distribution of the electrons (a) and of the protons of beam 2 (b) at  $t\Omega_e = 10^3$ : The colour scale shows the 10-logarithm of the number of CPs. The electrons display a plateau distribution for  $x/\lambda_u > 10$  and vortices for  $x/\lambda_u < 8$ . The plateau is split at  $x/\lambda_u \approx 9$ . The proton beam shows tenuous filaments, which are protons trapped in the ion acoustic waves. A phase space hole is forming at  $x/\lambda_u \approx 9$ .

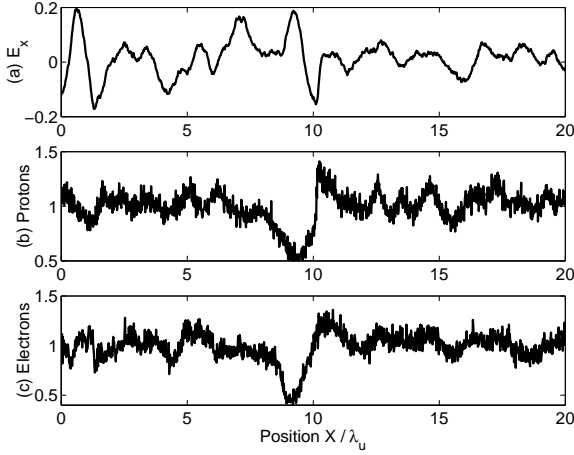


Fig. 5.— The normalized electrostatic field  $eE_x/(\Omega_e c m_e)$  (a), the proton density of beam 2 (b) and the electron density (c). The electric field shows a bipolar oscillation at  $x/\lambda_u \approx 9$ , which modulates the densities of the protons and electrons. The time is  $t\Omega_e = 10^3$ .

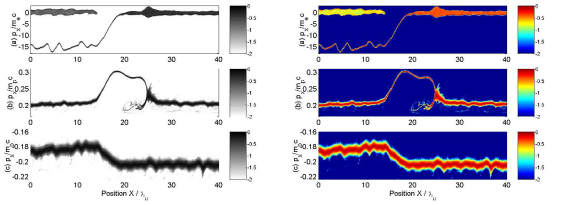


Fig. 6.— The phase space distributions at  $t\Omega_e = 2000$  of the electrons (a), the protons of beam 2 (b) and of beam 1 (c). The colour scale is the 10-logarithm of the number of CPs. The electron distribution evidences a double layer in the interval  $15 < x/\lambda_u < 20$ . The Double layer is maintained by the proton pulse moving with the beam 2, which is strong enough to modulate the protons of beam 1.

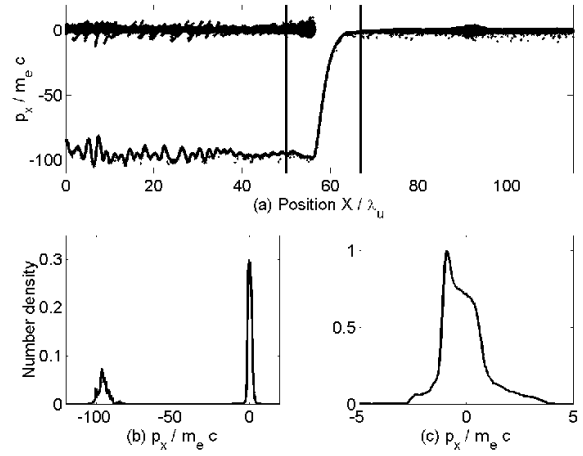


Fig. 7.— The electron distribution at  $t\Omega_e = 2600$ . The phase space distribution in (a) demonstrates that the width of the double layer is still  $5\lambda_u$ , but that the electrons reach now 50 MeV. The electron phase space distribution is integrated over the left interval  $x/\lambda_u < 50$  in (a) and the number density is plotted in (b). Two beams are visible. The integral over  $x/\lambda_u > 66$  in (c) shows a single electron beam.

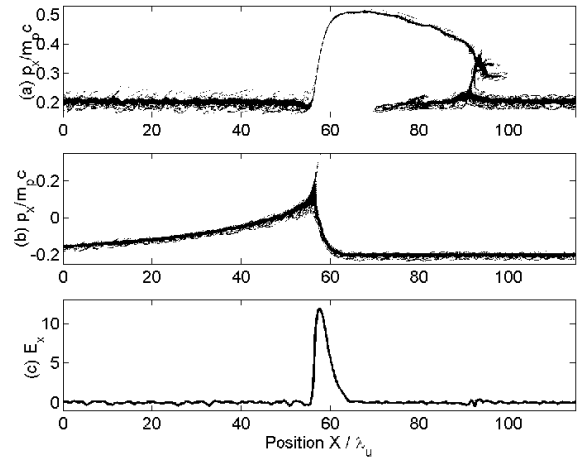


Fig. 8.— The proton distribution at  $t\Omega_e = 2600$  of beam 2 (a) and of beam 1 (b). Panel (c) shows the normalized electric field  $eE_x/(\Omega_e c m_e)$ . A large electrostatic shock is forming at  $x/\lambda_u \approx 55$ , which involves the protons of both beams. An electrostatic shock involving only the protons of beam 2 is driven by the rapid expansion of the pulse at  $x/\lambda_u \approx 92$ .

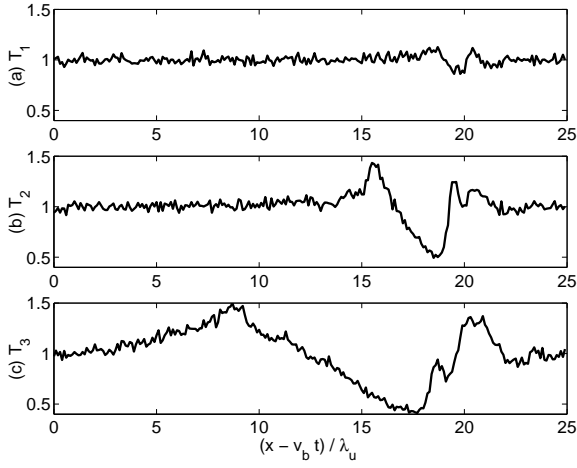


Fig. 9.— The oxygen density at the times  $t\Omega_e = 1000$  (a), at  $t\Omega_e = 1600$  (b) and  $t\Omega_e = 2000$  (c) in the reference frame convected with the proton beam 2. The location of the original proton phase space hole is at  $(x - v_b t) / \lambda_u \approx 20$ . The density is integrated over 3 grid cells to reduce the noise. The density in (a) shows a density depletion of the order of the number density fluctuations. The density in (b) is modulated by about 50% and it has expanded in size in (c). The density varies approximately linearly over a limited interval in (b) and in (c).